Anal Bioanal Chem (2003) 375 : 53–61
DOI 10.1007/s00216-002-1664-5

PAPER IN FOREFRONT

H. Stadler · M. Mondon · C. Ziegler

Protein adsorption on surfaces: dynamic contact-angle (DCA) and quartz-crystal microbalance (QCM) measurements

Received: 10 September 2002 / Revised: 27 October 2002 / Accepted: 28 October 2002 / Published online: 28 November 2002

Abstract Adsorption of the protein bovine serum albumin (BSA) on gold has been tested at various concentrations in aqueous solution by dynamic contact-angle analysis (DCA) and quartz-crystal microbalance (QCM) measurements. With the Wilhelmy plate technique advancing and receding contact angles and the corresponding hysteresis were measured and correlated with the hydrophilicity and the homogeneity of the surface. With electrical admittance measurements of a gold-coated piezoelectrical quartz crystal, layer mass and viscoelastic contributions to the resonator's frequency shift during adsorption could be separated. A correlation was found between the adsorbed mass and the homogeneity and hydrophilicity of the adsorbed film.

Keywords Protein adsorption · Dynamic contact-angle analysis · Wilhelmy plate method · Quartz-crystal microbalance · Admittance measurement

Introduction

Protein adsorption on surfaces in a biological environment is the first step in biofilm formation and serves as a promoter for further bacterial adhesion [1]. The investigation of protein films and the knowledge of the mechanisms influencing it is an important area of research, as biofilms are relevant in many fields of medicine, food processing, and engineering. The processes and influences involved are still not fully understood as protein adsorption on surfaces is a phenomenon accompanied by a very complex change of different physical surface parameters. These parameters include topography, wetting behavior, surface charge, and mechanical stiffness. Most methods implemented for adsorption studies [2] are monitoring only a small selection of physical parameters. Optical methods, e.g. ellipsometry and surface plasmon resonance follow the changes in refractive index and thickness. Electrochemical methods like cyclic voltammetry and impedance spectroscopy are sensitive to changes in permeability, dielectric properties, and thickness of the adsorbed layer. The variations in free surface energy are accessible by contact angle measurements, the amount or mass of the adsorbed surface species can be investigated by fluorescence or radiolabelling assays or by gravimetric methods based on acoustic wave devices [3]. Two prerequisites of reliable protein adsorption studies may be defined.

1. To study the kinetic process of protein adsorption on the surface the applied technique has to be suited for liquid environment and dynamic time-resolved measurements.
2. To account for the variety of influencing parameters a combination of different measurement techniques is desirable.

In the present work two methods to investigate adsorption were compared in their independent response to a protein-surface model system. The well known serum albumin protein which is a major component to the total blood and saliva protein content was chosen as adsorbing species. For availability and cost reasons, the bovine serum albumin (BSA) analog to the human protein was employed. The model surface studied was gold which is of medical relevance.

With dynamic contact angle measurements changes in the homogeneity of surfaces exposed to protein solutions with different concentrations were monitored. It is possible to see the temporal development of the adsorption. The difference of the advancing and receding contact angles (hysteresis) is attributed to the homogeneity of the surface (see below).

The mechanical behavior of a surface film can be characterized via the resonant behavior of a QCM. The attenuation of the resonator's amplitude is correlated with the layer's viscosity. The frequency change is attributed to

H. Stadler · M. Mondon · C. Ziegler (✉)
University of Kaiserslautern, Department of Physics,
Erwin Schroedinger Str. 56, 67663 Kaiserslautern, Germany
e-mail: cz@physik.uni-kl.de

variations in the mass and elasticity of the adsorbate. Usually these effects are accessible only in combination. By applying certain model assumptions it is possible to separate the mass increase and the viscoelastic contribution (see below). Accordingly it is possible to monitor the surface coverage and the mechanical properties of the developing surface film dynamically and in situ.

Additionally it is shown in this work that the two physically different techniques offer results that are compatible with and complementary to each other: A mass increase on the surface is accompanied by homogenization of the surface.

Theoretical background

Principle of dynamic contact-angle analysis (DCA)

Contact angles give insight to the equilibrium of interfacial tensions. The interfacial tensions are the reversible work needed to change a surface under isothermal and isobaric conditions ($dW_{rev}=F_\gamma ds=\gamma dA$ resulting in $\gamma = \left(\frac{\partial W_{rev}}{\partial A}\right)_{T,p} = \left(\frac{\partial G}{\partial A}\right)_{T,p}$).

It can be represented as work per unit area or force per unit length.

According to the Young equation the relation between the solid/vapor (γ_{sv}), the solid/liquid (γ_{s1}), the liquid/vapor (γ_{1v}) interfacial tensions, and the contact angle θ of e.g. a droplet is given by:

$$\gamma_{sv} - \gamma_{s1} = \gamma_{1v} \cos\theta \quad (1)$$

The contact angle can also be determined indirectly by the Wilhelmy plate method [4], in which the specimen is dipped into a solution and the weight is measured for immersion and emersion. The microbalance measures a combination of the weight of the sample (mg), the interfacial– and the buoyancy forces $F_{buoyancy}$:

$$F = mg + L\gamma_{1v} \cos\theta - F_{buoyancy} \quad (2)$$

where L is the perimeter of the plate. Temporal resolution is achieved by running experiments with multiple cycles. With that changes in surface or solution composition can be monitored. This method can monitor changes on the timescale of minutes, as a typical time needed for one cycle. The formation of a biofilm from a protein solution takes place on the same timescale. On shorter time scales time-resolved static contact angles can be used to monitor surface changes [5]. The changes in this investigation are due to the adsorption of proteins on the surface forming a biofilm. Proteins may undergo conformational changes that allow hydrophobic residues to contact a hydrophobic surface ($\theta>90°$) exposing hydrophilic residues towards the solution. This results in a stronger bond between the protein and the surface [6, 7] and can lead to a more uniform and more hydrophilic surface chemistry.

Thermodynamically the advancing and receding contact angles should be equal. In real systems they often differ [8]. The origin of this difference can be attributed to surface inhomogeneities, as the intrinsic contact angle is only defined for flat, smooth, nonreactive surfaces [9]. The real contact angle can be described by different proportions of the surface (f_1 and f_2) that have different intrinsic contact angles (θ_1 and θ_2) resulting from chemical or topographical inhomogeneities according to Cassie [10, 11]: $\cos\theta_{real}=f_1 \cos\theta_1+f_2 \cos\theta_2$.

The difference between the advancing θ_{adv} and receding θ_{rec} contact angles is described as hysteresis: $\Delta\theta=\theta_{adv}-\theta_{rec}$. This hysteresis is determined by factors including the distribution of the different portions of the surface that act as barriers. It is a measure for the homogeneity of the surface. The more homogeneous a surface is, the smaller is the hysteresis. In measurements of advancing and receding contact angles the advancing contact angle is more sensitive to the change in high contact angle regions if most of the surface exhibits low contact angles. The opposite is true for the receding contact angle [10, 11]. The change in hysteresis can occur when the surface structure is reorganized and changes occur through, e.g., adsorption processes.

Principle of the quartz-crystal microbalance (QCM) technique

Piezoelectric crystals are excited to ultrasonic vibrations by applying alternating voltages on opposite crystal faces. Depending on substrate material, geometry, and crystal orientation different acoustic modes can be selected ranging from bulk, surface and plate modes to compressional and shear waves [12].

The most commonly used device is the so called quartz-crystal microbalance (QCM). It consists of a thin single-crystalline α-SiO_2-disc with an electrode pair on the upper and lower side for electrically contacting the crystal and for generating an acoustic shear wave in the bulk quartz material. Frequency and amplitude of the shear wave depend on the mechanical properties of the quartz crystal and its surface. Loading one electrode with a wave guiding medium results in frequency and amplitude changes. For a pure thin mass-layer rigidly coupled to the electrode Sauerbrey [13] derived a linear relation between mass change and frequency shift. A pure Newtonian liquid leads to a frequency shift dependent on liquid viscosity and density according to Kanazawa's equation [14]. Additionally, energy loss occurs resulting in a decrease of the resonator's quality factor and amplitude [15].

A more detailed description of the electromechanical behavior of a loaded QCM [16, 17, 18, 19] shows that the mechanical properties are represented in the electrical quartz impedance and admittance. The exact expression of the loaded quartz impedance as demonstrated in Ref. [20] is quite complicated. Near resonance approximations can be applied relating simple lumped electrical elements with measurable quantities like frequency shift $\Delta\nu$ and resonance resistance shift ΔR.

The admittance $Y=G+i\cdot B$ of the loaded QCM corresponds to a Lorentzian type spectrum. Real and imaginary

parts named conductance G and susceptance B can be written as

$$G(\nu) = G_{\max} \cdot \left[1 + \left(Q \frac{\nu^2 - \nu_{\max}^2}{\nu \cdot \nu_{\max}}\right)^2\right]^{-1} \quad (3)$$

$$B(\nu) = 2\pi \cdot C_0 \nu - \left(Q \frac{\nu^2 - \nu_{\max}^2}{\nu \cdot \nu_{\max}}\right) \cdot G(\nu) \quad (4)$$

The maximum G_{max} of G meets the mechanical resonance frequency ν_{max} of the compound oscillator comprised of unperturbed quartz and surface load on the electrode. Q is the quality factor of the loaded QCM, C_0 is the geometric capacitance of the quartz and ν is the frequency of the alternating excitation voltage.

A possible mechanical model of a protein adsorbate on a surface in liquid is a combination of a viscoelastic thin layer and a semiinfinite viscous medium. Additional important effects containing multiple layer formation and slippage of neighboring layers are treated in Ref. [21]. For monolayer formation assumed primarily relevant for this work one can refer to the thin-layer approximation of a single viscoelastic layer derived in Ref. [22]. The resulting frequency shift $\Delta\nu_{L-M}$ of the resonator is expressed as:

$$\begin{aligned}\Delta\nu_{L-M} &= \Delta\nu_{mass} + \Delta\nu_{viscoelastic} \\ &= -M \cdot (\Delta R_{L-M})^{1/3} - V \cdot \Delta R_{L-M}\end{aligned} \quad (5)$$

where $\Delta\nu_{L-M}=\nu_{layer+medium}-\nu_{medium}$ and $\Delta R_{L-M}=R_{layer+medium}-R_{medium}$ are the frequency and resistance differences between the liquid loaded quartz plus layer and the liquid loaded quartz without layer. The first term in Eq. (5) corresponds to the adsorbate mass and the second term to the adsorbate viscoelasticity. The two parameters M and V contain properties of the quartz crystal and the viscoelastic layer:

$$M = C_1 \cdot \left[\frac{\rho_L \mu_L^2}{\mu_L''}\right]^{1/3} \quad V = C_2 \cdot \frac{\mu_L'}{\mu_L''} \quad (6)$$

where C_1 and C_2 are two quartz constants of no further importance. Note that M depends on the density ρ_L and the viscoelastic properties of the layer represented in a complex shear module $\mu_L = \mu_L' + i \cdot \mu_L''$ with elastic part μ_L' and viscous part μ_L'' while V depends only on the viscoelastic properties of the adsorbate.

Measuring multiple frequency and resistance pairs of the QCM during protein adsorption in liquid enables one to separate the mass from the viscoelasticity of the adsorbed layer without further experiments by fitting the measured values with the model Eq. (5) and recalculating the mass term $\Delta\nu_{mass} = -M \cdot (\Delta R_{L-M})^{1/3}$ and the viscoelastic term $\Delta\nu_{viscoelastic} = -V \cdot \Delta R_{L-M}$ separately. An absolute determination of layer mass $\Delta m_{layer} = A \cdot \rho_L d_L$ and viscoelastic loss factor $\tau_{layer} = \mu_L''/\mu_L'$ requires the knowledge of the electrical and mechanical parameters of the individual quartz crystal, which can be obtained by calibration measurements. As this is not in the scope of the present work, these considerations are not elaborated here.

Experimental

Materials

Gold wire (purity 99.99%) with a diameter of 1 mm was obtained from Degussa AG, Germany. It was used as coating material for QCM and as substrate for DCA.

AT-cut circular shaped blank quartz crystals with a fundamental resonance frequency of 10 MHz and a diameter of 8.5 mm were obtained from RSG Electronic Components GmbH, Germany.

Bovine serum albumin (BSA, fraction V powder, approx. 99%) was obtained from Sigma–Aldrich Chemie GmbH, Germany. Sodium dodecyl sulfate (SDS, >99.0%) was bought from Merck KGaA, Germany. The water for the solutions was deionized to a resistance of 18 MΩ and purified to a total organic content below 10 ppb using a Millipore Q-Synthesis system (Millipore GmbH, Germany).

Phosphate-buffered solutions (0.1 mol L^{-1}) were prepared from K_2HPO_4 and KH_2PO_4 >99%, obtained from Fluka Chemie AG, Switzerland

Aqueous and phosphate-buffered protein solutions were prepared from a stock solution of 10 g L^{-1} BSA by dilution.

Dynamic contact angle measurements

The dynamic contact angle measurements were performed with the Dynamic Contact Angle Meter and Tensiometer DCAT11 (Dataphysics, Germany) based on the Wilhelmy plate method. Data were evaluated with the software SCAT11 supplied by the manufacturer.

The gold substrate was fastened with a clip at the microbalance. The vessel containing the solution was moved towards the substrate and the measurement started upon the first contact. This point is defined as immersion depth 0. From there the sample was advanced further with a dipping velocity of 0.2 mm s^{-1} down to an immersion depth of 10 mm and retracted to 0 mm thereafter. Ten cycles were recorded for each protein concentration. The total time of one adsorption experiment was accordingly 8 min. Aqueous and phosphate-buffered protein solutions were investigated. The values for calculation of the hysteresis were taken at the immersion depth of 8 mm as at this point an equilibrium is established. The recorded weight was converted into force per wetted length via correction by the perimeter of the substrate and the difference of the values for advancing and receding curves calculated for hysteresis analysis. With this value it is possible to compare measurements more easily.

Quartz-crystal microbalance measurements

Preparation of the quartz crystals

Quartz crystals were coated with a 5 nm adhesive titanium layer followed by 80–100 nm gold in a high-vacuum evaporation system (Labovac Drewa opt 400, Dresdner Vakuumtechnik, Germany) providing a large working electrode (diameter 7 mm) centered on the liquid side crystal face and a small electrode (diameter 5 mm) centered on the air side crystal face. The obtained gold surfaces were polycrystalline with an average roughness of 2–5 nm as checked by scanning force microscopy. The gold coated and electrically contacted quartz crystals were annealed in an oven at 120 °C for 60 min. Prior to their use in adsorption measurements they were rinsed with Milli-Q-water and dried in N_2 to remove dust particles.

Flow-through setup

The quartz crystals were mounted in a fluid cell. The fluid cell (measurement volume 40–50 µL) was designed to expose only the larger working electrode to the fluid, to allow for a continuous

flow of liquid across the quartz surface, to avoid air bubbles in the measurement chamber and to assure a proper electrical contact with the measuring instruments. Liquid flow through the measurement cell was maintained by a peristaltic pump (model Reglo Analog, Ismatec Laboratoriumstechnik GmbH, Germany) at flow rates of about 100 μL min^{-1}. Flow inside the liquid chamber was directed against gravity to avoid pressure spikes on the vibrating crystal and to drive out air bubbles. The electrodes were contacted from the liquid free backside by spring contacts which were integrated in a click-on adapter supporting a cable connection to the measuring instrument.

Admittance spectroscopy

In this work, real and imaginary parts of the quartz admittance were measured because they allow an easy separation of the interesting mechanical branch from the geometrical and stray capacitances of the quartz holder and the electrical contacts.

Instrumentation. For a.c.-measurements a network analyzer (model Advantest R3753AH, delivered by Rhode & Schwarz GmbH, Germany) was used. The admittance was investigated in transmission by connecting the output source and signal input of the analyzer to the quartz working and backside electrodes, respectively. The home made measuring bridge consisted of a shielding aluminium box containing the quartz fluid cell. The instrument outside the box was linked to the quartz via isolated BNC-connectors (fixed in the wall of the box) and a cable adaptor with two pins contacting the electrodes.

Calibration. The measurement bridge was calibrated in the desired frequency range by a three point-procedure: The open-condition was approximated by leaving the bridge unconnected, the short-condition by connecting a copper wire and the load-condition by connecting a 50-Ω resistor. The network analyzer corrected the measured data by internal routines using the three calibration points. The quality of calibration was checked by measuring the frequency of the admittance maximum of an encapsulated reference quartz with a given resonance frequency of 10.000 MHz (housing HC49/U, RS Components, Germany). The measured frequency deviated by less than 0.04% from the reference.

Measurement procedure. The electrical admittance of the quartz was measured continuously in a small frequency band around the fundamental resonance. Center frequency and bandwidth were adjusted dynamically to the real part of the resonance curve: The measurement band was always centered at the conductance maximum with a frequency span set to three conductance bandwidths. Each admittance spectrum consisting of the conductance G and the susceptance B was taken with a measurement filter of 100 Hz in about 3 s at 301 equidistant frequency spots.

The admittance measurements were controlled by a PC (90 MHz Pentium) running on Windows 95 (Microsoft GmbH Deutschland, Germany). For data acquisition software based on the graphical user interface HP Vee 4.0 (Agilent Technologies Deutschland, Germany) was developed. This program automatically and continuously detected the frequency and bandwidth of the quartz vibration and adjusted the measurement as described above. Baseline corrected real and imaginary parts G and B of the admittance were fitted with the Lorentzian spectrum as formulated in Eqs. (3) and (4) which gives the resonance admittance G_{max}, the resonance frequency ν_{max}, the quality factor Q of the quartz vibration, and the geometrical capacitance C_0. A relative fitting error was calculated by comparing the measured raw data with the fitted admittance data and was always below 0.1%. The continuously extracted parameters ν_{max}, G_{max}, Q, and C_0 were stored digitally with the elapsed time measurement since the start for further data analysis.

Adsorption studies

To monitor protein adsorption on gold, the flow cell containing a gold-coated quartz crystal was continuously and slowly flushed with water (fluid inlet connected with a water reservoir, fluid outlet connected with a peristaltic pump). Water was replaced by freshly prepared BSA-solutions of different concentrations, followed again by pure water to completely remove the protein solution and to desorb weakly bound molecules from the surface. Prior to the next protein solution the gold surface was regenerated with 0.1 mol L^{-1} SDS solution and water. In a set of adsorption experiments protein solutions where analyzed in order of increasing protein content.

Results and discussion

Dynamic contact angle measurements

With the dynamic contact angle measurements a reduction in hysteresis was observed for all experiments. This change can be attributed to the formation of a protein layer. Control measurements in pure water with phosphate-buffered solution show no reduction in hysteresis after the initial change from the dry to the wetted surface. In Fig. 1 a typical curve is shown. Indicated is the development of the advancing angle with constant receding angle leading to a reduction in hysteresis, and the immersion depth at which the data analysis was done.

All changes appear in the advancing contact angle with the receding staying at a constant level (Fig. 1). The advancing angles change to more hydrophilic behavior. This change indicates a hydrophilization of the surface due to the protein adsorption.

The reduction in hysteresis and hydrophilization shows that by adsorption of the protein the small amount of hydrophobic parts of the surface is being reduced and an overall hydrophilization and homogenization occurs upon adsorption. Proteins are able to undergo conformational changes and hence to adsorb on hydrophobic as well as on hydrophilic surfaces. In the above case this leads to an en-

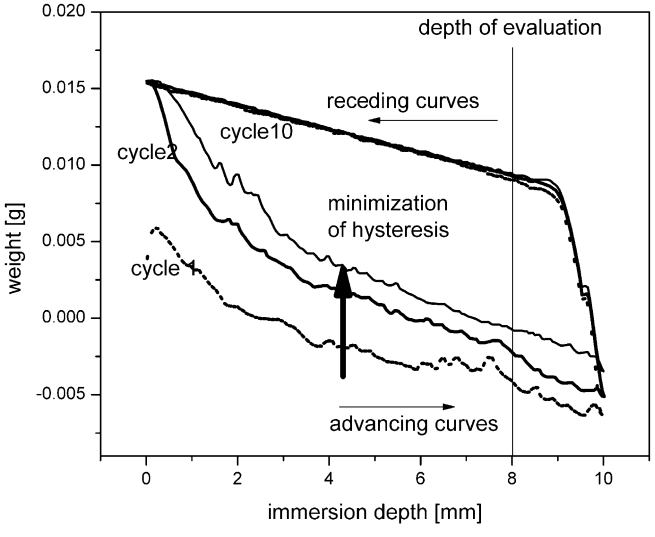

Fig. 1 Typical measurement of an adsorption with the minimization of hysteresis. For clarity cycles 1, 2, and 10 only are shown. Evaluation of the data was done at 8 mm immersion depth

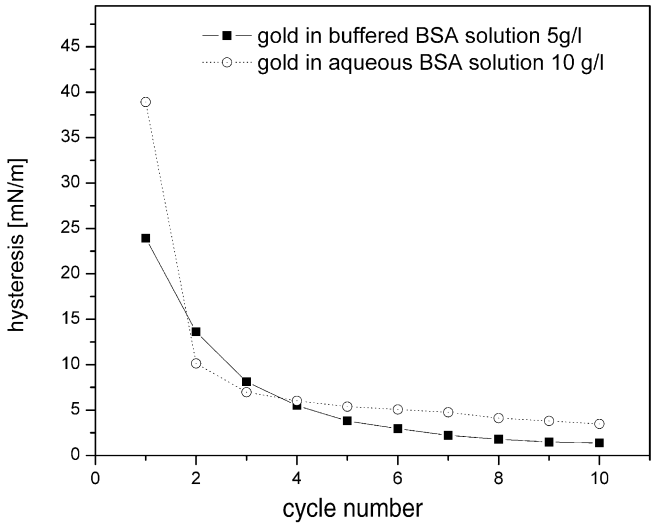

Fig. 2 Temporal changes in hysteresis over the 10 cycles of adsorption

ergetically favorable system with hydrophilic residues exposed towards the solution.

The hysteresis approaches a steady state during the 10 cycles indicating saturation and an equilibrium between the proteins in the solution and those in the surface layer (Fig. 2).

The final hysteresis is a function of the concentration and diminishes with increasing concentration. At concentrations of 10 g L^{-1} BSA the hysteresis approaches a steady value close to zero resulting in the fact that higher concentrations do not yield further information. This could be characterized by the formation of a monolayer. As could be shown in QCM experiments no further adsorption is taking place. This behavior towards the concentration c can be modeled by a Langmuir fit:

$$f(c) = B\left[1 - \frac{c}{A + c}\right] \tag{7}$$

with B as constant for the initial value and $A = 1/K_{Lang}$ resulting in a Langmuir constant K_{lang} of 5.5 L g^{-1} (Fig. 3).

The hysteresis changes occurring in aqueous solution are different to those in phosphate-buffered solution. In aqueous solution the hysteresis is generally higher than in the buffered solution. The influence of the phosphate buffer homogenizes the surface. This influence is further enhanced by the adsorption of proteins to yield at higher concentrations a homogeneous surface. The hysteresis in phosphate-buffered solutions reaches this homogeneity close to 5 g L^{-1} whereas the protein adsorption in aqueous solution approaches a steady value close to zero hysteresis at 10 g L^{-1}.

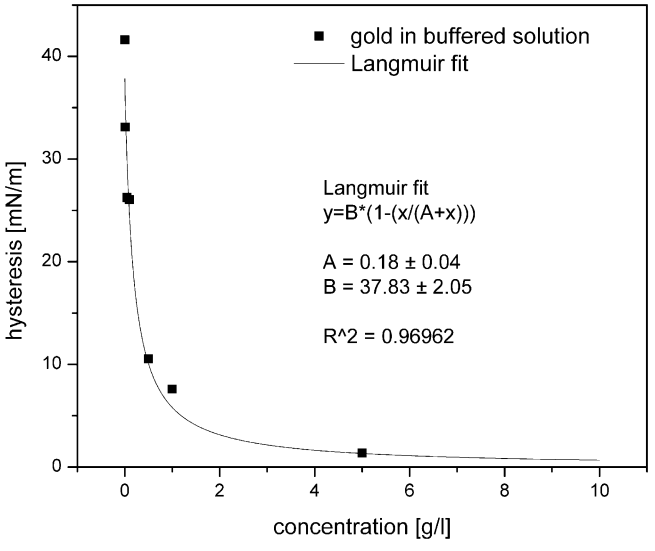

Fig. 3 Dependency of the hysteresis on the BSA concentration in buffered solution

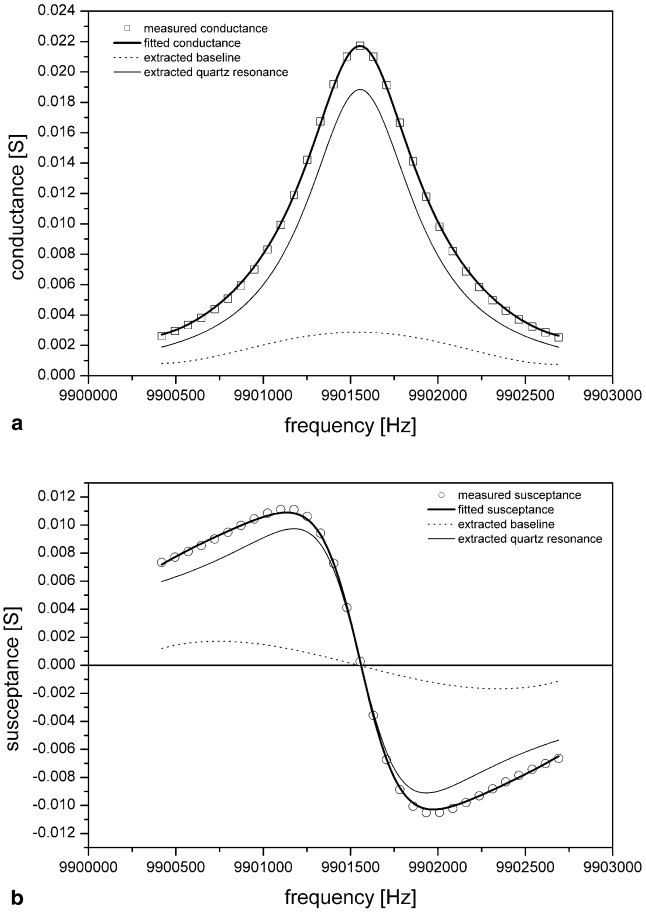

Fig. 4 (**a**) Real part (conductance) and (**b**) imaginary part (susceptance) of the electrical admittance measured with a quartz crystal gold coated in-house. Baseline correction and resonance curve extraction are plotted as well. For clarity, only each tenth measured data point is displayed

Table 1 Resonance parameters of a commercially available reference quartz (10.000 MHz) and a quartz crystal coated with gold in-house

	ν_{max} (Hz)	G_{max} (mS)	Q	C_0 (pF)
Reference quartz	9,996,938.98	147.62	111,283.68	2.032
Gold-coated quartz	9,901,554.55	18.84	13,074.45	5.082

Quartz-crystal microbalance measurements

Quartz characteristics

The admittance of a gold coated quartz crystal in air is shown in Fig. 4.

The extracted resonance parameters are compared in Table 1 to those of an encapsulated reference quartz which was used to calibrate the network analyzer.

The frequency shift of the gold coated quartz corresponds to a coating mass [13] of 85±43 µg assuming a fundamental frequency of 10±0.05 MHz as specified by the manufacturer and taking mechanical quartz properties from the literature [23]. This implies a gold layer with a thickness of 112±57 nm which is in the expected range.

The quality factor of the gold-coated quartz is far below the quality factor of the reference quartz which points out additional internal friction within the quartz bulk or the coating layer, and to perturbations from the surrounding medium possibly based on:

1. slight deviations from the theoretical AT-cut and clamping effects generating a non-pure shear motion and leading to energy loss by compressional wave radiation;
2. friction at domain boundaries within the polycrystalline coating layer; and
3. temperature effects and air humidity under non-ideal ambient conditions inducing additional dissipative stress on the electrode surface.

Nevertheless, the in-house coated quartzes could well be used in adsorption experiments.

Protein adsorption onto gold

During adsorption of BSA onto gold, frequency and resistance of the resonator are changing characteristically (Fig. 5a).

The adsorption process is accompanied by a decrease of the resonance frequency and an increase in resonance resistance. Once the protein solution reaches the measurement cell, the adsorption is completed within about 2 min. As was seen in desorption experiments with pure water (data not shown), BSA adsorbs irreversibly on gold which might be due to the formation of covalent sulfur–gold linkages explaining the high affinity to the gold surface. Regeneration with 0.1 mol L^{-1} SDS-solution for about 5 min could remove the adsorbate layer in most cases (mean baseline shift of –2.83 Hz and 0.14 Ω in N=12 subsequent adsorption and regeneration steps). Saturation of frequency and resistance during protein flow-through could be achieved after 15 min in all experiments. Plotting the saturation values in dependence of the BSA-concentration yields a monotonically increasing surface loading characteristic (Fig. 5b).

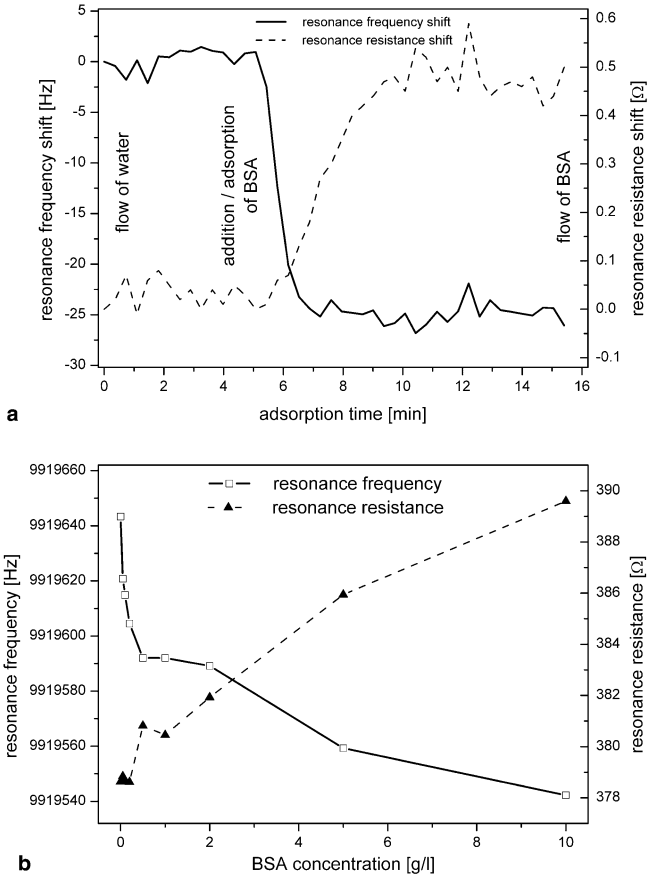

Fig. 5 (**a**) Time dependence of resonance parameter shifts during injection of BSA solution (0.5 g L^{-1}) into the liquid cell (kinetic measurement). (**b**) Concentration dependence of resonance parameters near saturation (15 min after injection)

This data set is further processed as explained in the next section.

Viscoelastic correction of frequency shifts

To separate viscoelastic effects from the pure mass increase on the resonator's surface the relationship between frequency shift and resistance can be examined as described in Sec. 2.2. The fit of the model function to the Δν–ΔR data of a series of kinetic BSA adsorption measurements is exemplarily demonstrated for three concentrations in Fig. 6.

It should be noted that BSA solutions with concentrations below 5.0 g L^{-1} do not induce resistance changes larger than 4 Ω in the given experimental data. In this low-load regime all data including the protein solutions with the highest contents can be explained very well with

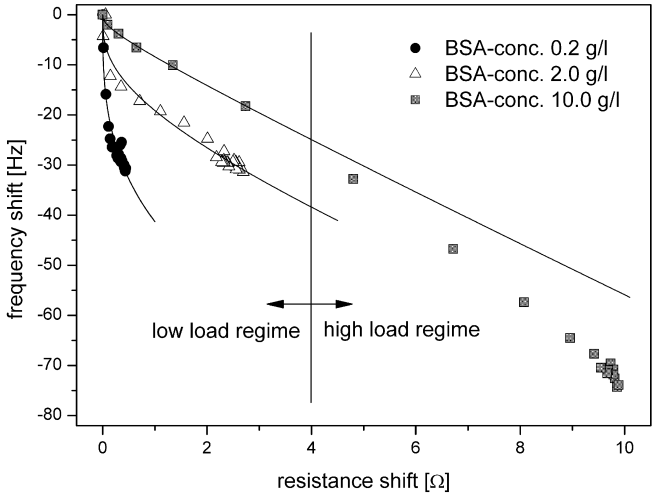

Fig. 6 Modelling the protein layer as a viscoelastic load with discrete lumped elements for viscoelasticity and mass. For clarity, only three concentrations are displayed

the suggested viscoelastic model. In the high-load regime a significant deviation occurs indicating additional contribution to quartz stiffness or inertia resulting in lower frequencies as proposed by the model at the same value of the resonance resistance. The excess frequency shifts obtained for BSA-concentrations of 5.0 g L^{-1} and 10.0 g L^{-1} are proportional to the resonance resistance with different slopes (-4.19 Hz Ω^{-1} and -2.85 Hz Ω^{-1}, respectively). This excludes a mass effect from a theoretical point of view (Eqs. 5 and 6). On the other hand, a pure viscous effect would not vary the slope of the $\Delta\nu$–ΔR curve upon changes in nature or concentration of the liquid. It is feasible to assume that in higher concentrated macromolecular solutions the liquid medium itself shows viscoelastic behavior, at least in a boundary layer attached to the adsorbate on the surface. Another possible explanation is a change in the viscoelasticity of the protein layer during adsorption leading to a kink in the $\Delta\nu$–ΔR relationship. The assumption of viscoelasticity variations due to conformational changes near a surface is often applied to explain the resonant behavior of a biomacromolecule-loaded QCM [24, 25] including molecule swelling or shrinking because of absent or present charge screening in low or high ionic-strength electrolytes, respectively, and water migration into the porous biofilm structure. For the experimental data in this work, an unique attribution to one of the mentioned mechanisms cannot be given at the moment.

The model parameters M and V, and the separated saturation frequency shifts due to mass and viscoelasticity according to Eqs. (5) and (6) are summarized in Table 2. The mass term is calculated by subtracting the viscoelastic contribution to frequency ($\Delta\nu_{visc}$) from the experimental frequency shift, $\Delta\nu_{mass,corr} = \Delta\nu_{exp} - \Delta\nu_{visc}$.

Analogously to the surface hydrophilization and homogenization measured by DCA, the mass increase on the surface measured by QCM can be described by a Langmuir isotherm (experimental Langmuir constant of

Table 2 Viscoelastic model parameters obtained for adsorption onto gold from different BSA-solutions. The viscoelastic and mass contribution to frequency shift are tabulated as well

BSA conc. (g L^{-1})	M (Hz/$\Omega^{1/3}$)	V (Hz Ω^{-1})	$\Delta\nu_{visc}$ (Hz)	$\Delta\nu_{mass,corr}$ (Hz)
0.05	28.03	2.70	–0.55	–22.01
0.10	39.25	2.31	–0.09	–28.37
0.20	41.28	0.00	0.00	–38.83
0.50	30.35	1.60	–3.50	–47.79
1.00	13.64	2.60	–4.72	–46.59
2.00	15.77	3.34	–11.00	–43.17
5.00	5.35	3.83	–27.95	–56.06
10.00	3.56	4.82	–52.87	–48.24

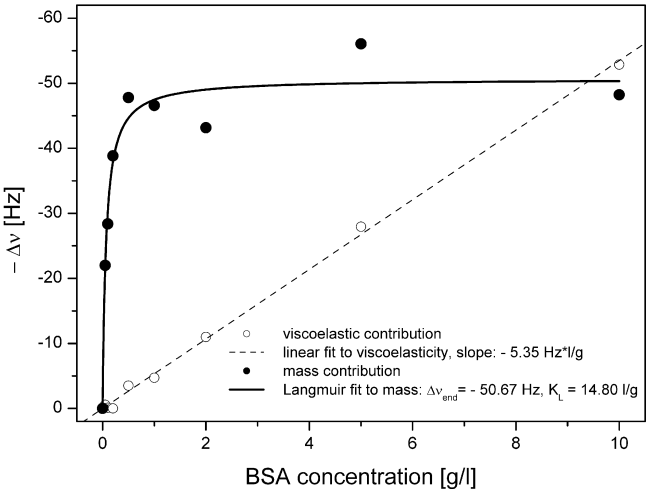

Fig. 7 Separation of mass and viscoelastic effect during adsorption of BSA

14.80 L g^{-1}; Fig. 7). The maximum mass uptake of the surface given by the plateau frequency shift amounts 44.7 ng which is about 15% larger than one BSA-monolayer of side-on oriented molecules (a complete coverage of the active electrode area with ellipsoidal shaped BSA-molecules of axis lengths 14×4×4 nm^3 yields 39.0 ng in side-on configuration, and 173.8 ng in end-on configuration). This deviation might be due to packing inhomogeneities within the surface layer, when molecules are arranged with different tilt angles with respect to the surface resulting in a higher packing density. Additionally, the viscoelastic term grows linearly with the BSA concentration which is due to layer stiffening when layer elasticity is enlarged relative to layer viscosity (Eq. 6). Possibly at higher protein concentrations the adsorbate layer formation is completed in an earlier stage of the experiment leading to a denser protein film compared to lower concentrations. In this case the protein film has enough time and molecular contact points to surface and neighbor molecules to reorganize and optimize intra- and extra-layer interactions.

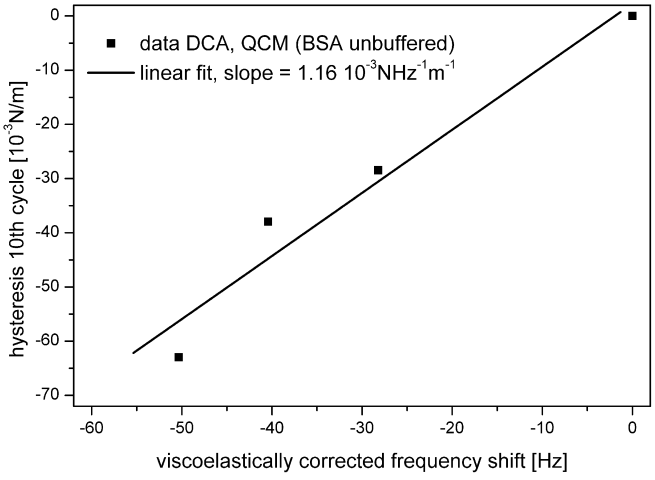

Fig. 8 Combination of hysteresis changes measured by DCA and the frequency shift measured by QCM. Both measurements were performed in unbuffered aqueous solution

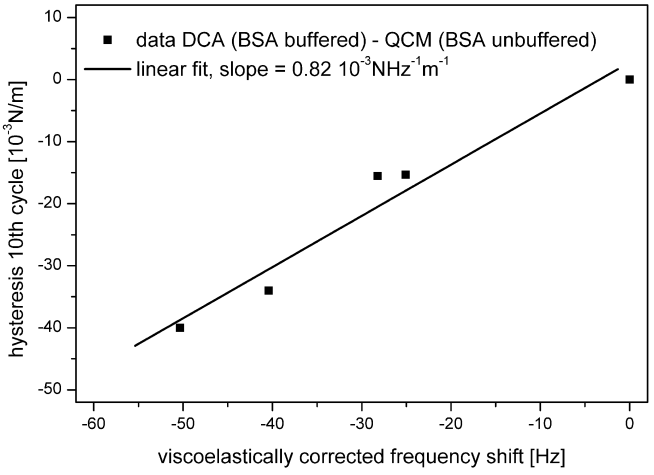

Fig. 9 Combination of hysteresis changes measured by DCA and the frequency shift measured by QCM. The DCA-measurement was performed in phosphate buffered solution, QCM was performed in unbuffered aqueous solution

Correlation of DCA and QCM

The relation between final hysteresis shifts taken from a DCA-measurement series and viscoelastically corrected frequency shifts taken from a QCM-measurement series in pure aqueous BSA solutions is depicted in Fig. 8.

The DCA-values are corrected with the value of a reference measurement in protein-free water.

A reasonable linear correlation ($r^2 = 0.95$) between the two data sets is obtained.

Figure 9 shows another comparison of DCA- and QCM-experiments. The hysteresis shifts resulting from a DCA-adsorption study in phosphate-buffered protein solutions with the reference measurement in pure buffer subtracted are related to the corrected frequency shifts of the corresponding QCM experiments in unbuffered protein solution.

Again, the linear dependency ($r^2 = 0.95$) is obvious.

The linear correlation in pure aqueous solution between reduction in hysteresis and frequency implies that a change in surface homogeneity is related to a mass change. This clearly confirms the assumption that temporal variations in wetting behavior measured with DCA during protein adsorption are actually due to formation of a protein layer on the surface. On the other hand, the identification of the adsorbed protein as a real surface mass with the sophisticated QCM admittance setup can be verified by the complexity of chemical and topographical information about surface state changes which are summarized in a hysteresis decrease.

The linear dependency between DCA of buffered protein solution and QCM of unbuffered protein solution might reflect a similar hysteresis decrease with increasing mass loading in presence of buffer salts. For a quantitative comparison of the two regression slopes pointing to a stronger effect in the unbuffered case one has to assume that the surface mass coverage is not drastically dependent on buffer conditions. This is questionable and has to be investigated separately.

Conclusion and outlook

In this work, dynamical contact angle and quartz-crystal microbalance experiments were employed to characterize the adsorption of bovine serum albumin onto gold surfaces in aqueous media. Both methods reveal saturation behavior at higher concentrations, showing up in a homogenized surface in a monolayer with a defined mass. Conformational changes of the protein at the surface are associated with the hydrophilization of the surface, represented by decreasing surface energy with decreasing advancing contact angles. Beside the changes in wetting behavior an increase in layer stiffness was found from QCM admittance measurements possibly due to restructuring effects during adsorption.

A major scope of this study was to investigate if the two independent measurement techniques for protein adsorption led to compatible results. For BSA in water the mass change and the chemical and topographical homogenization at the surface are clearly correlated. Interestingly, an additional linear relationship could be obtained by comparing hysteresis measurements in phosphate-buffered solutions and unbuffered QCM-measurements. The phosphate-buffered solution shows earlier homogenization but a smaller overall hysteresis change. If mass loading is assumed to be less influenced by buffer, these results indicate different surface homogeneity at the same mass loading in water and buffered solution.

The first results to our knowledge on combining QCM and DCA presented here are promising, and will stimulate further experimental work to apply this correlation for other protein-surface systems. A systematic variation of the medium composition, the protein species, and the sur-

face modification may lead to a more detailed understanding of the interface region between a biological fluid and a biomaterial.

Acknowledgements This work was partly supported by the Deutsche Forschungsgemeinschaft (project Zi 487/8) and by the "Stiftung Rheinland Pfalz für Innovation". The help of M. Strack with the coating of the quartz crystals and with the fluid cell construction is highly appreciated.

References

1. Gristina AG (1987) Science 237:1588–1595
2. Ramsden JJ (1993) Quart Rev Biophys 27:41–105
3. Kaspar M, Stadler H, Weiss T, Ziegler C (2000) Fresenius J Anal Chem 366:602–610
4. Wilhelmy L (1863) Ann Phys 119:177–217
5. Mondon M, Ziegler C (2003) Int J Prosth, in press
6. Chen X, Patel N, Davies MC, Roberts CJ, Tendler SJB, Williams PM, Davies J, Dawkes AC, Edwards JC (1998) Appl Phys A 66:S631–S634
7. Kidoaki S, Matsuda T (1999) Langmuir 15:7639–7646
8. de Gennes PG (1985) Rev Mod Phys 57:827–863
9. Wolansky G, Marmur A (1999) Colloids Surf A 156:381–388
10. Johnson RE, Dettre RH (1964) J Phys Chem 68:1744–1750
11. Dettre RH, Johnson RE (1965) J Phys Chem 69:1507–1515
12. Grate JW, Frye GC (1996) In: Baltes H, Göpel W, Hesse J (eds) Sensors update. sensor technology – applications – markets. Wiley–VCH, Weinheim, pp 37–83
13. Sauerbrey G (1959) Z Phys 155:206–222
14. Kanazawa KK, Gordon JG (1985) Anal Chem 57:1770–1771
15. Rodahl M, Höök F, Kasemo B (1996) Anal Chem 68:2219–2227
16. Rosenbaum JF (1988) Bulk acoustic wave theory and devices. Artech House, Boston
17. Martin SJ, Granstaff VE, Frye GC (1991) Anal Chem 63:2272–2281
18. Granstaff VE, Martin SJ (1994) J Appl Phys Appl Phys 75: 1319–1329
19. Bandey HL, Martin SJ, Cernosek RW, Hillman AR (1999) Anal Chem 71:2205–2214
20. Lucklum R, Hauptmann P (1997) Faraday Discuss 107:123–140
21. McHale G, Lucklum R, Newton MI, Cowen JA (2000) J Appl Phys Appl Phys 88:7304–7312
22. Wolff O, Seydel E, Johannsmann D (1997) Faraday Discuss 107:91–104
23. Lucklum R, Behling C, Cernosek RW, Martin SJ (1997) J Phys D 30:346–356
24. Su H, Thompson M (1996) Can J Chem 74:344–358
25. Rodahl M, Höök F, Fredriksson C, Keller CA, Krozer A, Brzezinski P, Voinova M, Kasemo B (1997) Faraday Discuss 107:229–246